Molecularly imprinted polymer as a synthetic receptor mimic for capacitive impedimetric selective recognition of Escherichia coli K-12

Nabila Yasmeen, Mathieu Etienne, Piyush Sindhu Sharma, Sofiane El-Kirat-Chatel, Mariela Brites Helú, Wlodzimierz Kutner

Analytica Chimica Acta 1188 (2021) 339177

Contents lists available at ScienceDirect

Analytica Chimica Acta

journal homepage: www.elsevier.com/locate/aca

Molecularly imprinted polymer as a synthetic receptor mimic for capacitive impedimetric selective recognition of *Escherichia coli* K-12

Nabila Yasmeen [a], Mathieu Etienne [b, **], Piyush Sindhu Sharma [a, *], Sofiane El-Kirat-Chatel [b], Mariela Brites Helú [b], Wlodzimierz Kutner [a, c]

[a] *Institute of Physical Chemistry, Polish Academy of Sciences, Kasprzaka 44/52, 01-224, Warsaw, Poland*
[b] *Université de Lorraine, CNRS, LCPME, F-54000, Nancy, France*
[c] *Faculty of Mathematics and Natural Sciences, School of Sciences, Institute of Chemical Sciences, Cardinal Stefan Wyszynski University in Warsaw, Wóycickiego 1/3, 01-815, Warsaw, Poland*

HIGHLIGHTS

- *E. coli* E2152 was successfully imprinted in a polymer by 2-aminophenylboronic acid and aniline co-electropolymerization.
- The bacteria template was entrapped in the resulting molecularly imprinted polymer in a single step.
- Thus prepared MIP film-based electrochemical chemosensor determined *E. coli* E2152 up to 2.9×10^4 cells/mL.
- *E. coli* E2152 determination was selective versus bacteria of other surface properties.

GRAPHICAL ABSTRACT

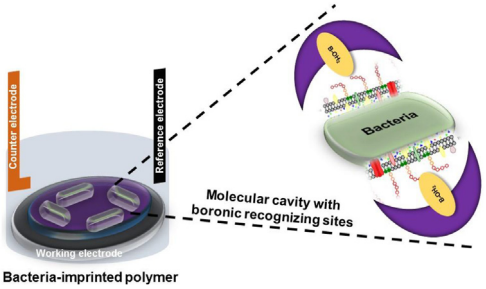

ARTICLE INFO

Article history:
Received 9 August 2021
Received in revised form
2 October 2021
Accepted 13 October 2021
Available online 14 October 2021

Keywords:
Escherichia coli K-12
Type 1 *fimbriae*
Ag43 protein
Shewanella oneidensis MR1
Capacitive impedimetry (CI) chemosensor
Bacteria imprinted polymer

ABSTRACT

We fabricated an electrochemical molecularly imprinted polymer (MIP) chemosensor for rapid identification and quantification of *E. coli* strain using 2-aminophenyl boronic acid as the functional monomer. This strain is a modified Gram-negative strain of *Escherichia coli* bacterium, an ordinary human gut component. The *E. coli* strongly interacts with a boronic acid because of porous and flexible polymers of the cell wall. The SEM imaging showed that the bacteria template was partially entrapped within the polymeric matrix in a single step. Moreover, this imaging confirmed *E. coli* K-12 cell template extraction effectiveness. The prepared MIP determined the *E. coli* K-12 strain up to 2.9×10^4 cells mL^{-1}. The interference study performed in the presence of *E. coli* variants expressing different surface appendages (type 1 *fimbriae* or Antigen 43 protein) or *Shewanella oneidensis MR1*, another Gram-negative bacteria, demonstrated that the bacterial surface composition notably impacts sensing properties of the bacteria imprinted polymer.

* Corresponding author.
** Corresponding author.
E-mail addresses: mathieu.etienne@univ-lorraine.fr (M. Etienne), psharma@ichf.edu.pl (P.S. Sharma).

https://doi.org/10.1016/j.aca.2021.339177

1. Introduction

One of the most recent food-related epidemic occurred in 2011 when a bacterial epidemic caused by enterohemorrhagic *Escherichia coli* (EHEC) strains spread to Germany, and several adjacent countries, leading to a European health crisis [1,2]. This epidemic mainly affected children resulting in hundreds of death across Europe [1]. Epidemiological studies have shown that the fatal infections were caused by virulent strains of *E. coli* belonging to a rare serotype defined by its ability to produce Shiga toxin [3,4] and its enhanced propensity to adhere to the digestive mucosa [5]. Rapid detection is a powerful strategy to prevent such an outbreak.

Several analytical methods using colorimetric analysis, polymerase chain reaction (PCR), enzyme-linked immunological assay (ELISA), and mass-spectrometry techniques are already quite well developed to quantify pathogenic and non-pathogenic microorganisms [6–8]. However, replacing these laborious and expensive molecular approaches with robust, convenient, and cost-effective sensing systems remains the top challenge. The conventional antibody-antigen host systems that determine pathogenic microorganisms lack specificity and stability towards the cell wall in these microorganisms [9]. Moreover, the global mortality rate because of pathogenic infections is rapidly growing worldwide. Therefore, a massive improvement is required in pre-existing sensing systems to limit infectious outbreaks [10]. The surface properties of bacteria that promote adhesion and infectiosity could also be derived for their detection by a sensor with an adequately tuned sensitive surface.

The molecularly imprinted polymers (MIPs), sometimes referred to as "artificial antibodies," are now established as readily accessible tools for identifying and quantifying macromolecular compounds like proteins, membrane glycolipids, and even whole bacteria cells [11,12]. MIP preparation is fast and inexpensive [13–16], and the synthesis procedure defines MIP properties [17]. Therefore, a growing emphasis is on improving MIP chemosensors design for selective targeting microbial surface functionalities [18–20]. The main requirement is to generate in MIPs and control the accessible imprinted cavities featuring recognizing sites. Generally, that is accomplished in classical bulk imprinting using cross-linking monomers in amounts sufficiently high to ensure the MIP stability. However, another way around is the surface imprinting, including the formation of thin nanofilms featuring a high surface density of imprinted cavities and low heterogeneity with geometrical constrictions fewer than bulk imprinting. This strategy provides a high control over the imprinting, enabling the effective template removal and binding of the target analyte in MIP nanofilms [21–26]. The MIP thin film-coated electrodes were recently excessively prepared to serve as electrochemical chemosensors to determine the DNA, rRNA, surface proteins, and pathogens exotoxins [27–29].

However, these procedures for recognizing bacterial components require a higher infectious dose and extra reagents for sample processing, which increases the cost and time for adequate diagnosis [30,31]. Therefore, the chemosensors sensing the whole microorganisms are more desirable for rapid testing [31–33]. Indeed, the encapsulation of whole bacteria cells provides an efficient way to imprint all microbial features present on the microbial surface, including antigenic properties, genomic elements, as well as all biochemical, electromechanical, and morphological features potentially beneficial for the fast and effective determination of specific microorganisms in a given sample [33].

In the present work, we aim to devise and fabricate an electrochemical MIP chemosensor for rapid identification and quantification of specific *E. coli* K-12 strain using 2-aminophenyl boronic acid (2-APBA) as the primary functional monomer and aniline (ANI) as the cross-linking monomer. We have used a modified Gram-negative strain of *Escherichia coli* bacterium, an ordinary human gut component. The *E. coli* strongly interacts with this conductive polymer. That is because of porous and flexible polymers of the cell wall structure. This bio-polymer feature is widely exploited for sensing purposes [34]. MIPs prepared using (boronic acid)-functionalized monomers gain attention mainly as a potential synthetic alternative to classical antibodies [35]. Moreover, hydroxyl groups of boronic acid may covalently react with *cis*-diols of the negatively charged glycoproteins to form five- or six-membered cyclic esters in an alkaline aqueous solution. Besides, these esters readily dissociate in an acidic solution [36–38]. Herein, we incurred selectivity to the MIP film prepared by applying the 2-APBA functional monomer reversibly binding glycan structures of the *E. coli* K-12 cell surface (Scheme 1).

2. Materials and methods

2.1. Bacterial strains

The *E. coli* K-12 strains were constructed from *Escherichia coli* MG1655 (*E. coli* genetic stock center CGSC #6300) by transforming the red linear DNA gene inactivation method using the pKOBEG plasmid [39]. All strains contained the gfpmut3 gene linked to the bla ampicillin-resistance gene (ampR, 100 g/mL) to make them fluorescent. In the present study, three mutants were used, vis., E2146, E2152, and E2498 expressing different surface appendages of different scales [39]. The surface of E2152 is less developed, with no type 1 fimbria and no antigen 43 (Ag43) protein. E2146 displays external ultrastructure type 1 fimbriae of the 1- to 10-μm length, and E2498 expresses a denser layer of the Ag43 protein with only 10-nm length. *Shewanella oneidensis* MR1 (ATCC 700550) was also used as interference for this study.

Tryptic soy broth (TSB), Luria-Bertani (LB), lysozyme, Triton X 100, sodium hydroxide NaOH, potassium chloride KCl, potassium hexacyanoferrate(III) $K_3[Fe(CN)_6]$, potassium hexacyanoferrate(II) $K_4[Fe(CN)_6]$, Tris-HCl buffer (pH = 7.4), 2-aminophenyl boronic acid (2-APBA) and aniline (ANI) purchased from Sigma Aldrich, were used as received.

2.2. E. coli K-12 growth conditions

The *E. coli* K-12 strains were pre-grown overnight for ~12 h in the LB broth at 37 °C and 160 rpm, in the presence of appropriate antibiotics to select the strains. The next day, a fresh culture was inoculated with that overnight pre-grown to an optical density of ~0.08, measured at 600 nm and then cultivated under the same conditions. The cultured bacteria cells were collected by triple centrifugation (5000 rpm for 10 min). Afterward, a pellet was collected and re-suspended in a sterilized 1 mM KCl. The same procedure was executed for the SWMR-1 strain except for the change in growth medium conditions characteristic for the strain used, i.e., the TSB broth at 30 °C.

2.3. Scanning electron microscopy

Scanning electron microscopy (SEM) imaging and energy-dispersive X-ray spectroscopy (EDS) spectra recording were performed on a JEOL JMS-IT500HR microscope (JEOL, Japan) equipped with the Ultim Max 170 EDS detector (Oxford Instruments, UK). The SEM images were taken with the 3–5 kV acceleration voltage at current emission of 35 μA and a working distance of 10 mm without coating the samples. EDS spectra were recorded for at least 30 s with an acceleration voltage of 5 kV and a working distance of 10 mm.

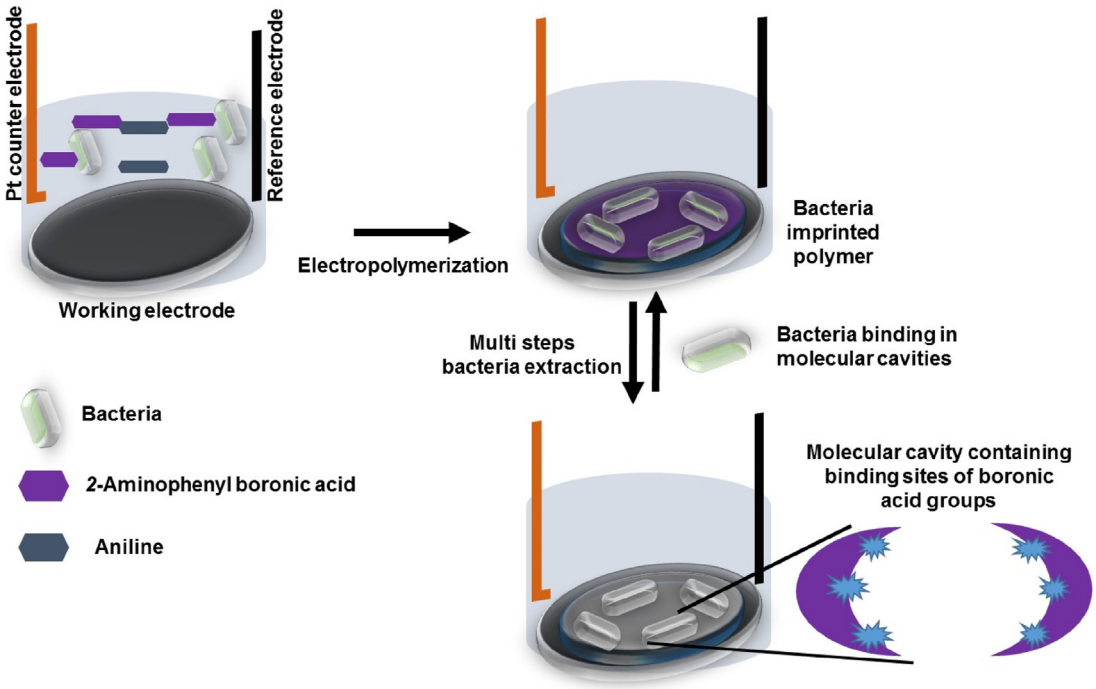

Scheme 1. The flowchart of *E. coli* E2152 imprinting by electro-copolymerization of aniline and *p*-aminophenylboronic acid in 0.01 M KCl on 7-mm diameter disk glassy carbon electrode.

2.4. Atomic force microscopy

Atomic force microscopy (AFM) imaging of the as-prepared, extracted, and *E. coli* bound MIP films were carried out using the Peak Force Tapping (PFT) mode with SNL-C tips. Images were obtained in the air using a Bioscope Resolve AFM microscope (Bruker).

2.5. Electrochemical polymerization

The electrochemical measurements were carried out with an SP-50 BioLogic potentiostat. The three-electrode cell system was used for simultaneous electropolymerizing and depositing (*E. coli*)-templated MIP films. A 7-mm diameter glassy carbon disk electrode, Pt wire coil, and an Ag/AgCl electrode (1 M KCl) were used as the working (WE), counter (CE), and reference (RE) electrode, respectively.

2.6. MIP film deposition

The E2152 strain was used as the template for molecular imprinting. 2-APBA and ANI were used as the functional and cross-linking monomers, respectively. The potentiodynamic technique was used for the MIP thin film deposition on the WE by cycling the potential between −0.20 and 1.10 V vs. Ag/AgCl at 25 mV s^{-1} in the 5-mL sample solution of 2.5 mM 2-APBA and 10 mM ANI monomers, and 0.01 M KCl supporting electrolyte, with a 200-μL sample of E2152 of optical density, OD 0.08 added.

3. Results and discussion

3.1. 2-APBA and ANI electropolymerization in the presence of E. coli E2152 cells

The multi-cyclic potentiodynamic curve in Fig. 1 represents electro-oxidation of the 2-APBA and ANI monomers in the presence

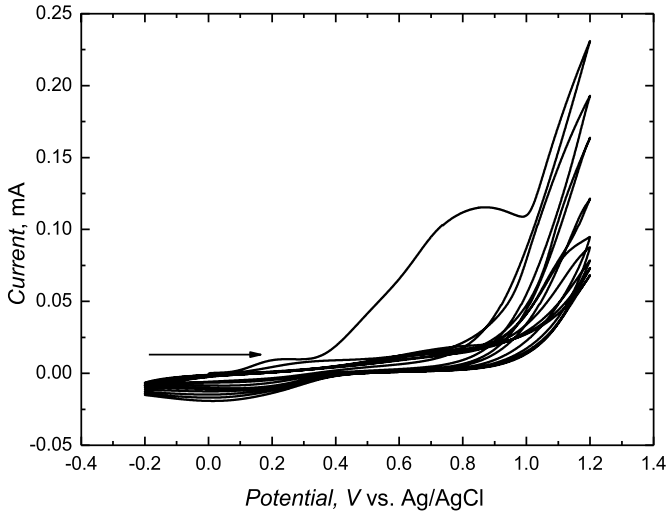

Fig. 1. The multi-cyclic potentiodynamic curve for the glassy carbon working electrode (0.38 cm^2) in the 5 mL 0.01 M KCl solution of 2.5 mM 2-APBA, 10 mM ANI, and 200 μL of E2152 suspension (5×10^9 cells mL^{-1}) at a scan rate of 25 mV s^{-1}. Currents decrease in consecutive cycles.

of the E2152 cells. A broad, irreversible anodic peak at ~0.85 V vs. Ag/AgCl corresponds to the electropolymerization of 2-APBA [40]. The non-conducting reduced leucoemeraldine form conversion into the conducting intermediate oxidized emeraldine form commenced at 0.20 V vs. Ag/AgCl. Subsequently, it changed into a fully oxidized pernigraniline form at 0.65 V vs. Ag/AgCl [41]. However, the appearance of only one anodic peak at 0.65 V vs. Ag/AgCl in successive cycles indicates the emeraldine-base form presence with a relatively low protonation and deprotonation rate in a neutral solution [42]. The potential was continuously cycled 12 times to deposit an MIP film capable of bacterial cells adhesion and entrapment in the polymer network.

3.2. Imagining of bacteria-imprinted MIP film

Bacteria cells partial covering with a polymer film evidences their successful imprinting. The AFM and SEM images clearly show effective E2152 capturing within the polymer network after electropolymerization (Fig. 2 and S1). The polymer layers partially covering the 3 μm long rod-shaped E2152 with a diameter of 0.8 μm are seen in the SEM (Fig. 2a, a', and S1) and AFM (Fig. 2b and b') images. During the electropolymerization, the boronic acid residues interact with the bacterial outer membrane diol-containing molecules, such as sugars [43]. That increases the cell adhesion to the polymer surface [44]. This reversible covalent affinity helped capture the bacteria cells within the MIP network during imprinting. Hence, after bacteria template removal, the MIP film was expected to recognize target bacteria by shape and size and molecular interactions between its boronic groups and surface glycoproteins of the bacteria.

Here the MIP film was prepared capable of recognizing bacteria concerning their size, shape, and surface groups. For that, MIP film prepared after 3, 6 and 12 electropolymerization cycles were surface imaged. After three cycles, the bacteria still stayed on top of a too-thin MIP film deposited (Fig. S2). After 12 cycles, overgrowth of an MIP film around the bacteria was seen (Fig. 2a, a'). Therefore, 12 cycles were used for the MIP film deposition.

3.3. Bacteria cells removing from the MIP film for emptying imprinted cavities

After MIP film preparation, several approaches were applied to remove bacteria for vacating imprinted cavities. Mild approaches, including soaking the bacteria-templated MIP film in an acidic or alkaline solution, appeared ineffective. Therefore, the following multistep extraction procedure was adopted. First, the MIP film was 2 h treated with 2 mg mL^{-1} lysozyme enzyme in PBS (pH = 7.4) for lysing the *E. coli* E2152 strain. The lysozyme helped break the intermolecular bonding of boronic acid residues of MIP with glycoproteins on the *E. coli* surface. The electrode was then immersed in 10% Triton X to remove the bacteria membrane debris and the lysozyme enzyme excess from the MIP film surface. Afterward, the MIP film was extensively rinsed with deionized water. Finally, it was overoxidized at +0.98 V vs. Ag/AgCl in 0.1 M NaOH for 20 min (Supporting Information, Fig. S3) to remove the bacteria cells completely. Each extraction step was monitored with SEM imaging. Electrodes coated with the bacteria-extracted MIP films were stored in 0.1 M PBS (pH = 7.4) until further use. The SEM and AFM images in Fig. 3a and 3a', and 3b show the complementary cavities formed because of efficient bacteria template removal from the MIP film. Worth mentioning, missing any extraction step resulted in no bacteria extraction (Supporting Information, Fig. S4).

3.4. ***Electrochemical characterizing (E2152)-templated and (E2152)-extracted MIP films***

Further, electrochemical impedance spectroscopy (EIS) and differential pulse voltammetry (DPV) were used to characterize the (E2152)-templated and (E2152)-extracted MIP film. Fig. 4a, 4b, and 4c show changes in the charge transfer resistance and DPV peak current, incurred by the presence of 5 mM $K_3[Fe(CN)_6]$ and 5 mM $K_4[Fe(CN)_6]$ in 0.1 M PBS (pH = 7.4), for the MIP film-coated electrode before and after bacteria removal. The MIP film charge transfer resistance determined from the Nyquist plot before bacteria extraction was high (Fig. 4a). Presumably, the E2152 cells entrapment in the film blocked the electron transfer between the redox probe molecules in the solution and the electrode substrate.

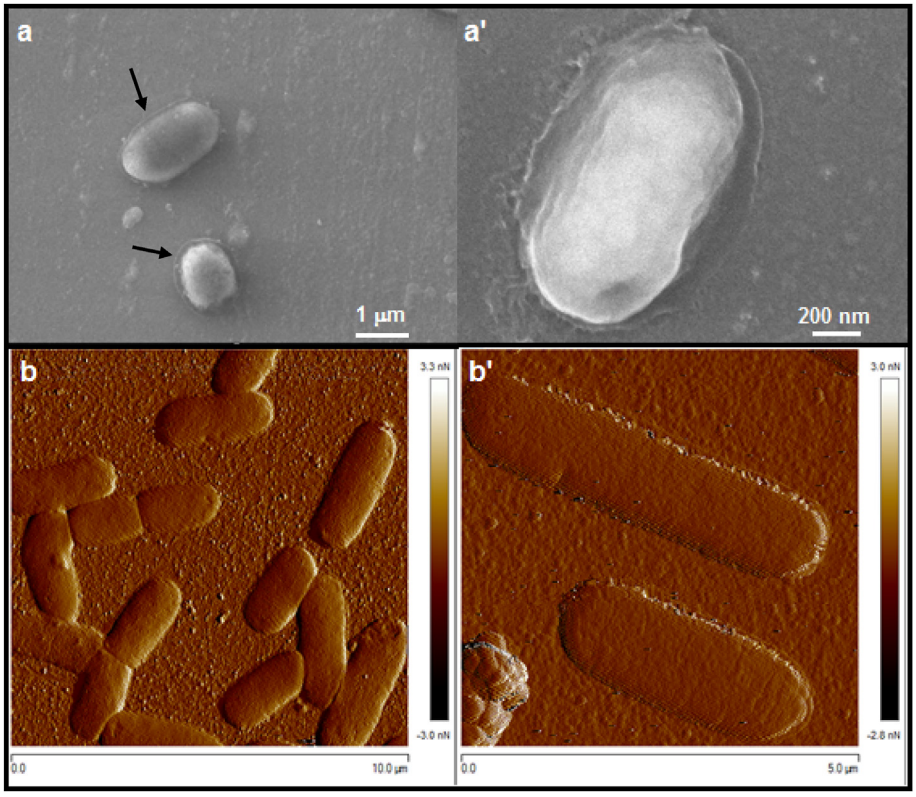

Fig. 2. (a, a') SEM and (b, b') AFM images of the glassy carbon electrode coated with the *E. coli* E2152 imprinted MIP film before washing. An MIP film was overgrown around the bacteria (shown with arrows in the SEM images).

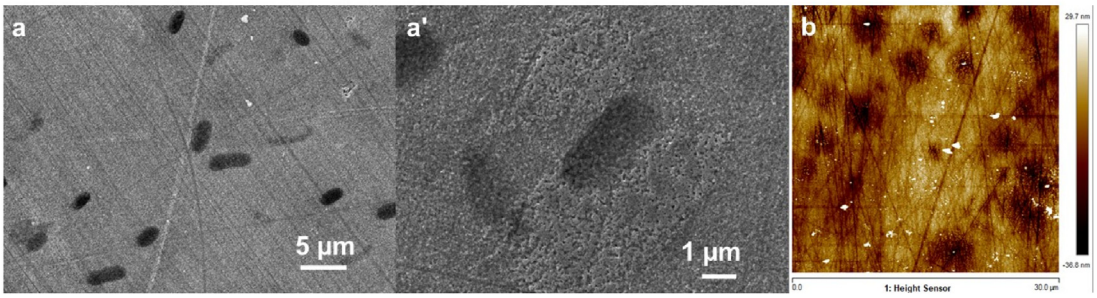

Fig. 3. (a, a') SEM image at two different resolutions and (b) the AFM image of the bacteria (E2152)-extracted MIP film-coated glassy carbon electrode.

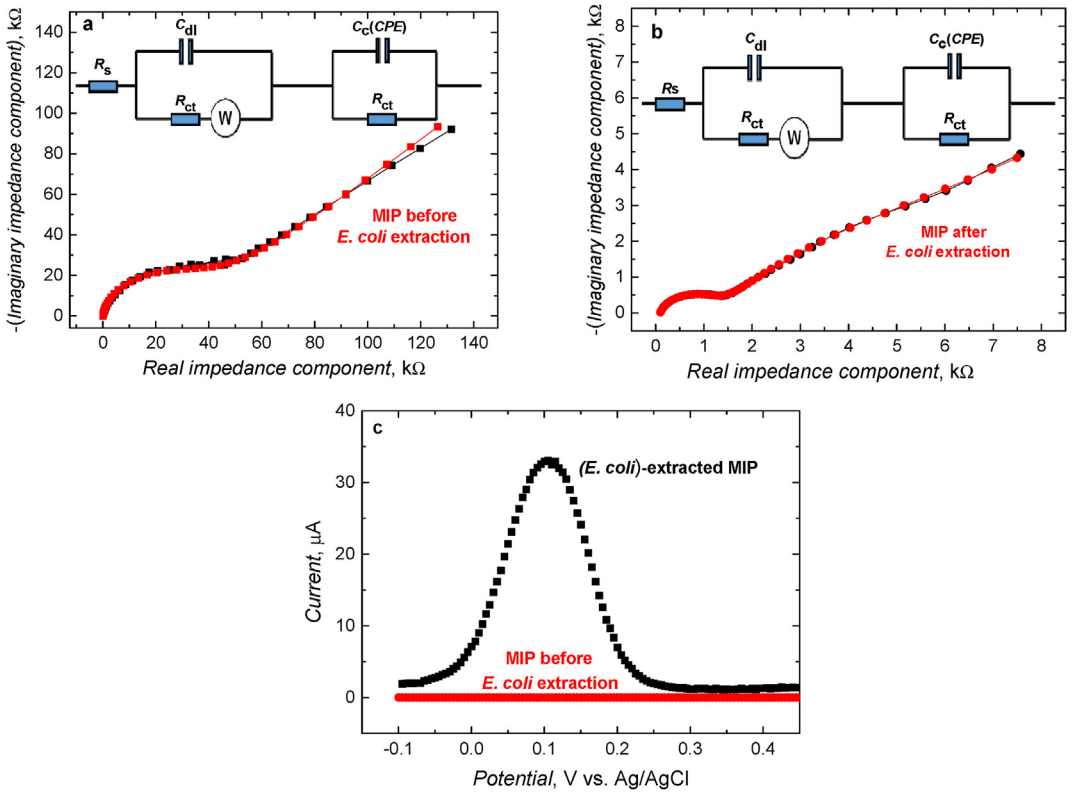

Fig. 4. The Nyquist plots for the (a) E2152-templated, and (b) E2152-extracted MIP film-coated electrode. (c) The DPV curves for the E2152-templated and E2152-extracted MIP film-coated electrode. All experiments were performed using 5 mM $K_4[Fe(CN)_6]$ and 5 mM $K_3[Fe(CN)_6]$ in 0.1 M PBS (pH = 7.4).

In contrast, the charge transfer resistance of this film-coated electrode with E2152 cells removed was relatively small (Fig. 4b). This removal resulted in the MIP film poration, causing the oxidation current of the redox probe to increase (Fig. 4c).

Moreover, insets to Fig. 4a and 4b propose equivalent circuits for the MIP film-coated electrode before and after, respectively, E2152 extraction. The solid curves represent the best-fit curves based on the proposed circuits. For the best simulation, two Randles circuits were connected in series to represent the contribution of the interface parameters, including bulk solution resistance (R_s), double-layer capacitance (C_{dl}), contact capacitance (C_c), the charge transfer resistance (R_{ct}), and a Warburg diffusion element (W) for the MIP film-coated glassy carbon electrodes. In the circuits, the C_{dl} and C_c, in parallel, are connected with R_{ct} to represent the faradic transport processes and the charge transfer kinetics of the redox probe ions transition at the polymer-electrolyte solution interface. Moreover, because of expected porosity in the MIP film, the pseudocapacitive element, vis., the constant phase element (CPE), represents the pure capacitive elements C_{dl} and C_c [45]. The determined R_{ct} value was 38.54 and 1.2 kΩ before and after extraction, respectively, for the MIP coated electrodes. This noticeable R_{ct} decrease after extraction appreciably contributed from encapsulated bacteria within the MIP film to double-layer capacitance. Moreover, the significant change in R_{ct} reflects the considerable increase in the diffusion rate of redox probe ions in the MIP-electrolyte interface because of the presence of MIP-imprinted cavities.

3.5. XPS analyzing (E2152)-templated and (E2152)-extracted MIP films

Surprisingly, the boron band is absent in the XPS spectrum of the MIP film before bacteria extraction. However, this band appears only after bacteria removal (Supplementary Information, Fig. S5), confirming the boron presence in bacteria stamps. The bacteria present in the film mask the boron band. A possible explanation can

come from the strong interaction of these residues with a bacterial surface that would induce a concentration gradient between the bacteria and the polymer; boron becoming then undetectable in the XPS analysis before extracting the bacterial cells and emptying the cavity (XPS depth of surface analysis is limited to ~10 nm).

3.6. Recognition efficiency of bacteria-templated MIP films

The MIP boronic acid residues are expected to interact with the bacterial outer membrane *cis*-diol surface groups reversibly during electropolymerization. This covalent affinity aids in capturing bacteria cells within the MIP network during imprinting. Therefore, it is anticipated that the MIP film after the bacteria template removal would recognize the target bacteria by shape and size and molecular interactions between MIP boronic acid residues and bacteria surface glycoproteins. The E2152-extracted MIP film-coated glassy carbon electrodes were used for *E. coli* determination by capacitive impedimetry (CI) under steady-state solution conditions.

For the *E. coli* EIS determination under steady-state solution conditions, the 100 mM Tris-HCl buffer (pH = 7.4) was used as the supporting electrolyte solution at the applied frequency and potential of $f = 20$ Hz and $E_{appl} = 0.60$ V vs. Ag/AgCl, respectively. The steady-state analysis first step is to attain the time-independent capacitance to confirm stable electric double layer formation at the electrode-solution interface. Afterward, the analyte is introduced to the test solution. The *E. coli* binding in molecular cavities is mainly governed by electrostatic attractions of positively charged *E. coli* surface groups and negatively charged porous MIP film boronic acid residues. This *E. coli* binding affects the electric permittivity of the electric double layer. Therefore, the capacitance and phase angle change with successive addition of *E. coli* of different concentrations (Fig. 5). The linear dynamic concentration range for the *E. coli* analyte extended from 2.9×10^4 to 3.1×10^7 cells mL^{-1} with the calibration plot obeying a semi-logarithmic linear regression equation of capacitance [nF] = 0.46(±0.04) [nF/log (cells mL^{-1})] × $c_{E.\ coli}$ [log (cells mL^{-1})] − 2.0(±0.19) (Supporting Information, Fig. S6). The correlation coefficient was $R^2 = 0.984$ while the sensitivity was 0.46(±0.04) [nF/log (cells mL^{-1})].

Moreover, *E. coli* E2152 binding was evidenced with SEM imaging of the *E. coli* E2152 extracted MIP film-coated electrode after adding the bacteria cells (Supplementary Information, Fig. S7). Expectedly, the cells mainly settled at the bacteria-imprinted cavities instead of the unimprinted MIP film surface (Supplementary Information, Fig. S7b). The bacteria binding was governed by the boronic acid residue present in the cavities, possible to detect with the XPS measurement only if the cavities were vacated (Supplementary Information, Fig. S5).

Gram-negative pathogens, including multidrug-resistant *E. coli* strains, are enclosed by an outer membrane, essential for cell viability and a protective barrier against antibodies. This asymmetric outer core comprises lipopolysaccharides (LPSs), phospholipids, and lipoproteins, playing a crucial role in sensing and antimicrobial activity [46]. The most abundant and vital structural lipoproteins covalently bound to the peptidoglycan layer via the ε-amino group are responsible for the outer core's stability and integrity. In comparison, the glycolipids and phosphorylated oligosaccharides (OS) are the major components of LPS making the strain highly hydrophobic [47]. However, the *E. coli* E2152 outer core is highly anionic because it is enriched with phosphate groups and 3-deoxy-D-manno-octulosonic acid and lacks O-polysaccharide. Because of this highly anionic surface nature, the boronic acid residues form *cis*-diol bonds with exposed glycolipids to firmly encapsulate the whole bacteria cell within the film during electropolymerization. Subsequently, the template-extracted MIP gains a positive charge because of the MIP film overoxidation during extraction in a highly alkaline solution (0.1 M NaOH). This cationic surface of the MIP helps bind the negatively charged *E. coli* E2152 into the imprinted cavities generated. Herein, this binding was transduced with CI. However, to confirm this hypothesis, the binding behavior of three interferences, namely, *Shewanella oneidensis* MR-1 (SWMR-1) and two *E. coli* strains, E2146 (with type 1 *fimbriae*), and E2498 (with Ag43 protein) were studied under steady-state conditions using the same test solution, namely, 100 mM Tris-HCl buffer (pH = 7.4) (Fig. 6). The interferences of known concentrations were separately added to the test solution under the same conditions for CI determination, i.e., the frequency and potential were kept constant at $f = 20$ Hz and $E_{appl} = 0.60$ V, respectively. The obtained results showed that the bacteria surface composition notably impacts the prepared MIP sensing properties.

As shown in Fig. 6, no changes in capacitance were found for the E2498 interference. Presumably, this arises from the presence of an additional dense peripheral thin layer of auto-transported adhesion Ag43 protein, a product of the flu gene on the *E. coli* K-12 chromosome, over the outer core of bacteria cell membrane [39]. *E. coli* Ag43 is a short and rigid monomeric appendage composed of a C-terminal integral outer membrane β domain that exports an *N*-terminal passenger α domain [48,49]. Interestingly, Ag43 variants display a twisted L-shaped β-helical structure that helps in the auto-aggregation and cell-cell interactions via a molecular "Velcro-type" mechanism [50]. At pH = 7.4, the Ag43 domains aggregation is at maximum [51]. Therefore, the drastic change induced on the bacterial surface by this bacteria auto-aggregations and additional coverage results in the lack of recognition that eventually appeared as no CI analysis response. Simultaneously, capacitance and phase angle pronouncedly changed for the E2146 mutant adsorption on the E2152-extracted MIP film. The E2146 mutant is composed of a rod-shaped 100- to 200-nm thick layer of partially bent fimbriae. Moreover, the repeating fimbriae subunits with lectin group endings play an essential role in biofilm formation and bacterial virulence [52]. The unwinding of these tiny fimbriae extensions increases with the pH increase and reaches a pronounced maximum elongation at pH = 7.4 [53]. This surface modification is much less dense than that with Ag43 expression of E2498 [39]. Therefore, it seems that the appreciable binding of E2146, comparable to E2152, might correlate to the more limited surface modification compared to E2498.

The third interference selected was Gram-negative SWMR-1, commonly known as metal-reducing bacteria externally surrounded by extracellular polymeric substances [54]. The EPS mainly comprises polysaccharides (~90%), including galactose, glucose, mannose, *N*-acetyl glucosamine, and glucuronic acids with smaller protein ratios, nucleic acids, and amyloid formations [55,56]. A very minute change in capacitance and phase angle values for just one higher concentration of SWMR-1 depicts that the binding is most likely dependent on the arrangement of exposed surface proteins and also on the surface charge density of binding agents, which in the case of Gram-negative SWMR-1 is smaller compared to *E. coli* K-12 strains [57,58].

During the imprinting of microbes, their surface groups play a role. Therefore, the proper selection of functional monomers was crucial in generating functionally adapted cavities. The excess of cross-linking monomer maintained the shape of the cavities after template removal from the MIP and helped functional monomers positioning in microcavities. Moreover, bacteria binding was controlled via electrostatic and hydrophobic interactions and reversible covalent bonding with boronic functional groups. That way, boronic diester saccharides complexes were formed. An SEM image (Fig. 3a) showed a well-defined fingerprint left after

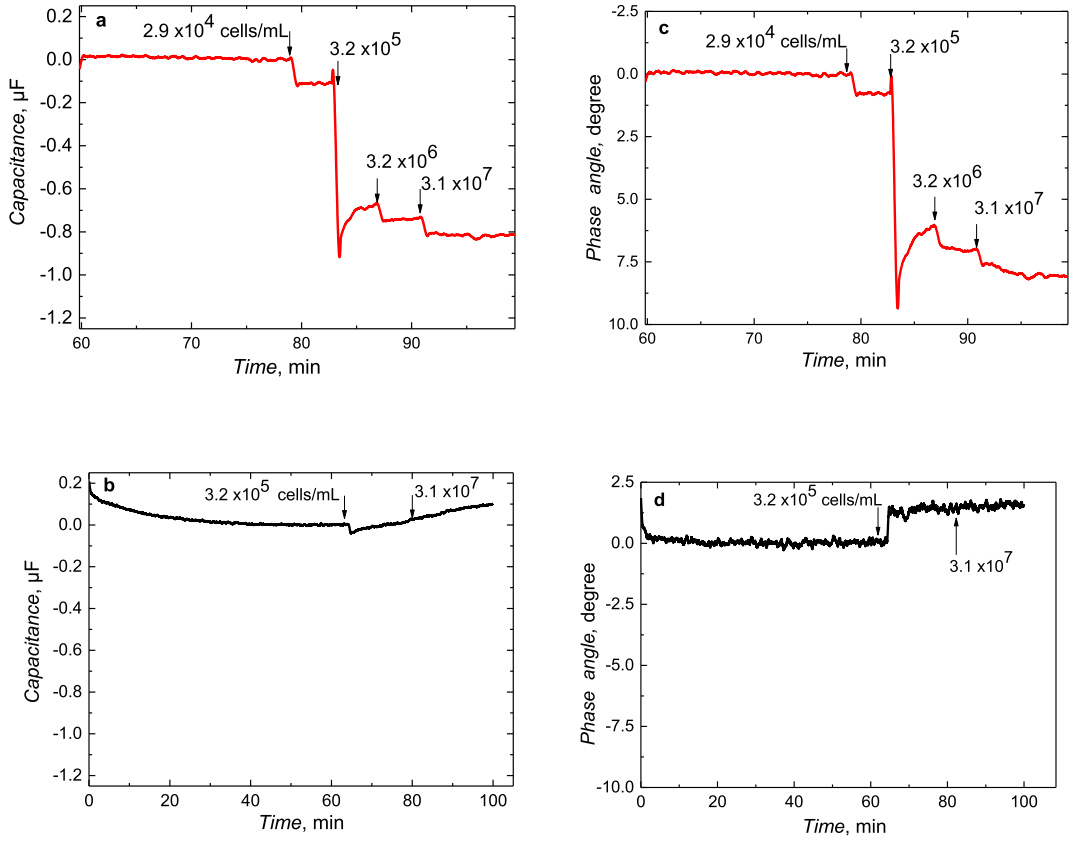

Fig. 5. The time dependence of changes of (a, b) capacitance and (c, d) phase angle after addition of *E. coli* E2152 of different concentrations to 100 mM Tris-HCl buffer (pH = 7.4) measured at the (a, c) E2152-templated MIP and (b, d) NIP film-coated electrodes under steady-state solution conditions. Electrodes were kept at the potential of +0.60 V vs. Ag/AgCl and frequency of 20 Hz.

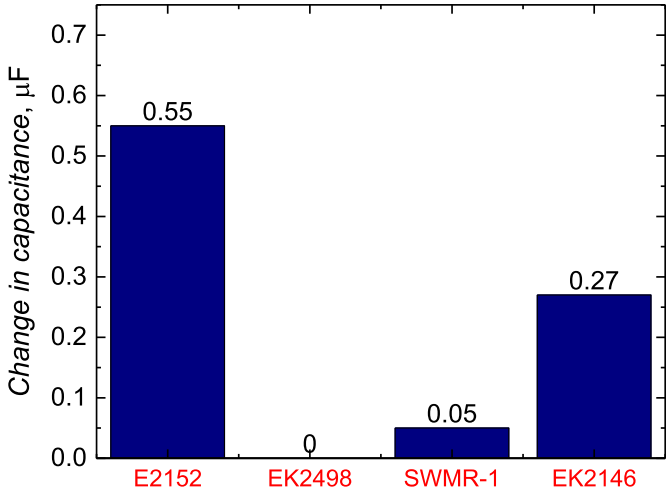

Fig. 6. Histograms of capacitance changes of the MIP film-coated glassy carbon electrode after addition of 3.2×10^5 cells mL^{-1} of E2152, E2498, SWMR-1, or E2146 to 100 mM Tris HCl buffer (pH = 7.4) under steady-state conditions. The electrode was kept at a constant potential of 0.60 V vs. Ag/AgCl and frequency of 20 Hz for capacitance measurements.

removing the imprinted *E. coli* single bacterium. Because of the presence of boronic functional groups and the size and shape of the cavities generated, the template entrapment by combined size-shape discrimination and affinity recognition was possible. All strains other than the template bacteria yielded low capacitance change, thus pointing out the unique recognition characteristics of cavities generated during molecular imprinting.

4. Conclusions

An *E. coli E2152* strain was successfully imprinted in a polymer using electrochemical polymerization. 2-Aminophenyl boronic acid was used as the functional monomer, along with aniline as the cross-linking monomer. The SEM images showed that the bacteria template was fully entrapped in the resulting molecularly imprinted polymer (MIP) matrix in a single step without any additional laborious steps. The adopted three-step procedure of generating MIP cavities appeared successful. Then, SEM imaging confirmed that the template extracting procedure was effective. The target *E. coli* E2152 strain was determined by MIP film-coated electrode up to 2.9×10^4 cells mL^{-1}. The interference study results indicated that the cell surface compositions mainly governed their binding behavior.

CRediT authorship contribution statement

Nabila Yasmeen: Methodology, Formal analysis, Data curation, Writing – original draft. **Mathieu Etienne:** Methodology, Supervision, Writing – review & editing. **Piyush Sindhu Sharma:** Conceptualization, Methodology, Data curation, Supervision, Funding acquisition, Writing – review & editing. **Sofiane El-Kirat-Chatel:** Formal analysis. **Mariela Brites Helú:** Formal analysis. **Wlodzimierz Kutner:** Supervision, Funding acquisition, Writing – review & editing.

Declaration of competing interest

The authors declare that they have no known competing financial interests or personal relationships that could have appeared to influence the work reported in this paper.

Acknowledgments

We thank Dr. Francius Grégory and Dr. Xie Wang for providing bacteria strains and initial training in growing the bacteria culture. We acknowledge Dr. Renard Aurélien (LCPME, France) for XPS analyses. The research activity of NY was financially supported by funds from the European Union's Horizon 2020 research and innovation program under the Marie Skłodowska-Curie grant agreement 711859and by financial resources for science in the years 2017–2021 awarded by the Polish Ministry of Science and Higher Education for the implementation of an international co-financed project.

Appendix A. Supplementary data

Supplementary data to this article can be found online at https://doi.org/10.1016/j.aca.2021.339177.

References

[1] E. Köckerling, L. Karrasch, A. Schweitzer, O. Razum, G. Krause, Public health research resulting from one of the world's largest outbreaks caused by enterohemorrhagic *Escherichia coli* in Germany 2011: a review, Front. Public Health 5 (2017) 332.
[2] O. Ergonul, F. Can, M. Akova, L. Madoff, Emerging infectious diseases: clinical case studies, in: O. Ergonul, F. Can (Eds.), Developments in Emerging and Existing Infectious Diseases, Academic Press, 2014.
[3] A. Caprioli, G. Scavia, S. Morabito, Public health microbiology of Shiga toxin-producing *Escherichia coli*, Microbiol. Spectr. 2 (2014) 1–12.
[4] J.B. Kaper, A.D. O'Brien, Overview and historical perspectives, Microbiol. Spectr. 2 (2014) 1–9.
[5] E.J. Boll, J. Ayala-Lujan, R.L. Szabady, C. Louissaint, R.Z. Smith, K.A. Krogfelt, J.P. Nataro, F. Ruiz-Perez, B.A. McCormick, Enteroaggregative *Escherichia coli* adherence fimbriae drive inflammatory cell recruitment via interactions with epithelial MUC1, mBio 8 (2017) e00717, 00717.
[6] X. Wang, X. Li, S. Liu, H. Ren, M. Yang, Y. Ke, L. Huang, C. Liu, B. Liu, Z. Chen, Ultrasensitive detection of bacteria by targeting abundant transcripts, Sci. Rep. 6 (2016) 20393.
[7] E. Galikowska, D. Kunikowska, E. Tokarska-Pietrzak, H. Dziadziuszko, J.M. Łoś, P. Golec, G. Węgrzyn, M. Łoś, Specific detection of Salmonella enterica and *Escherichia coli* strains by using ELISA with bacteriophages as recognition agents, Eur. J. Clin. Microbiol. Infect. Dis. 30 (2011) 1067–1073.
[8] T.N. Le, T.D. Tran, M.I. Kim, A convenient colorimetric bacteria detection method utilizing chitosan-coated magnetic nanoparticles, Nanomaterials 10 (2020) 92.
[9] A. Ahmed, J.V. Rushworth, N.A. Hirst, P.A. Millner, Biosensors for whole-cell bacterial detection, Clin. Microbiol. Rev. 27 (2014) 631–646.
[10] M.F. Alwashmi, The use of digital health in the detection and management of COVID-19, Int. J. Environ. Res. Publ. Health 17 (2020) 2906.
[11] S. Piletsky, F. Canfarotta, A. Poma, A.M. Bossi, S. Piletsky, Molecularly imprinted polymers for cell recognition, Trends Biotechnol. 38 (2020) 368–387.
[12] J. Pan, W. Chen, Y. Ma, G. Pan, Molecularly imprinted polymers as receptor mimics for selective cell recognition, Chem. Soc. Rev. 47 (2018) 5574–5587.
[13] Z. Iskierko, P.S. Sharma, K. Bartold, A. Pietrzyk-Le, K. Noworyta, W. Kutner, Molecularly imprinted polymers for separating and sensing of macromolecular compounds and microorganisms, Biotechnol. Adv. 34 (2016) 30–46.
[14] J. Kalecki, M. Cieplak, M. Dąbrowski, W. Lisowski, A. Kuhn, P.S. Sharma, Hexagonally packed macroporous molecularly imprinted polymers for chemosensing of follicle-stimulating hormone protein, ACS Sens. 5 (2020) 118–126.
[15] M.f. Jia, Z. Zhang, J. Li, X. Ma, L. Chen, X. Yang, Molecular imprinting technology for microorganism analysis, TrAC Trends Anal. Chem. (Reference Ed.) 106 (2018) 190–201.
[16] S.A. Zaidi, Bacterial imprinting methods and their applications: an overview, Crit. Rev. Anal. Chem. (2020), https://doi.org/10.1080/10408347.2020.1755822.
[17] L. Chen, S. Xua, J. Lia, Recent advances in molecular imprinting technology: current status, challenges and highlighted applications, Chem. Soc. Rev. 40 (2011) 2922–2942.
[18] Y. Zhang, K. Llapashtica, S. Shinde, B. Sellergren, Z. El-Schich, A.G. Wingren, Determination of cytokine regulated glycan expression by using molecularly imprinted polymers targeting sialic acid, J. Canc. Metastasis Treat. 5 (2019) 56.
[19] S. Shinde, Z. El-Schich, A. Malakpour, W. Wan, N. Dizeyi, R. Mohammadi, K. Rurack, A.G. Wingren, B. Sellergren, Sialic acid-imprinted fluorescent core-shell particles for selective labeling of cell surface glycans, J. Am. Chem. Soc. 137 (2015) 13908–13912.
[20] M.A.R. Khan, F.T.C. Moreira, J. Riu, M.G.F. Sales, Plastic antibody for the electrochemical detection of bacterial surface proteins, Sens. Actuators, B 233 (2016) 697–704.
[21] Z. She, K. Topping, M.H. Shamsi, N. Wang, N.W.C. Chan, H.-B. Kraatz, Investigation of the utility of complementary electrochemical detection techniques to examine the in vitro affinity of bacterial flagellins for a toll-like receptor 5 biosensor, Anal. Chem. 87 (2015) 4218–4224.
[22] F. Cui, Z. Zhou, H.S. Zhou, Molecularly imprinted polymers and surface imprinted polymers based electrochemical biosensors for infectious diseases, Sensors 20 (2020) 996.
[23] H. Ahari, M. Hedayati, B. Akbari-adergani, S. Kakoolaki, H. Hosseini, A. Anvar, Staphylococcus aureus exotoxin detection using potentiometric nanobiosensor for microbial electrode approach with the effects of pH and temperature, Int. J. Food Prop. 20 (2017) S1578–S1587.
[24] M. Amiri, A. Bezaatpour, H. Jafari, R. Boukherroub, S. Szunerits, Electrochemical methodologies for the detection of pathogens, ACS Sens. 3 (2018) 1069–1086.
[25] Y. Saylan, Ö. Erdem, N. Cihangir, A. Denizli, Detecting Fingerprints of waterborne bacteria on a sensor, Chemosensors 7 (2019) 33.
[26] J.G. Lopez, E.V. Piletska, M.J. Whitcombe, J. Czulak, S.A. Piletsky, Application of molecularly imprinted polymer nanoparticles for degradation of the bacterial autoinducer *N*-hexanoyl homoserine lactone, Chem. Commun. 55 (2019) 2664–2667.
[27] M.A.R. Khan, A.R.A. Cardoso, M.G. Sales, S. Merino, J.M. Tomás, F.X. Rius, J. Riu, Artificial receptors for the electrochemical detection of bacterial flagellar filaments from Proteus mirabilis, Sens. Actuators, B 244 (2017) 732–741.
[28] G. Gupta, P.K. Singh, M. Boopathi, D.V. Kamboj, B. Singh, R. Vijayaraghavan, Molecularly imprinted polymer for the recognition of biological warfare agent staphylococcal enterotoxin B based on surface plasmon resonance, Thin Solid Films 519 (2010) 1115–1121.
[29] S. Ramanavicius, A. Jagminas, A. Ramanavicius, Advances in molecularly imprinted polymers based affinity sensors (Review), Polymers 13 (2021) 974.
[30] P.G. Bowler, B.I. Duerden, D.G. Armstrong, Wound microbiology and associated approaches to wound management, Clin. Microbiol. Rev. 14 (2001) 244–269.
[31] H.-K. Huang, H.-W. Cheng, C.-C. Liao, S.-J. Lin, Y.-Z. Chen, J.-K. Wang, Y.-L. Wang, N.-T. Huang, Bacteria encapsulation and rapid antibiotic susceptibility test using a microfluidic microwell device integrating surface-enhanced Raman scattering, Lab Chip 20 (2020) 2520–2528.
[32] M.V. Lenti, C. Mengoli, M. Vernero, N. Aronico, L. Conti, F.B.d. Andreis, S. Cococcia, A.D. Sabat, Preventing infections by encapsulated bacteria through vaccine prophylaxis in inflammatory bowel disease, Front. Immunol. 11 (2020) 485.
[33] S. Ramanavicius, A. Ramanavicius, Conducting polymers in the design of biosensors and biofuel cells, Polymers 13 (2021) 49.
[34] S. Ghasemia, M.R. Baria, S. Pirsaa, S. Amirib, Use of bacterial cellulose film modified by polypyrrole/TiO_2-Agnanocomposite for detecting and measuring the growth of pathogenic bacteria, Carbohydr. Polym. 232 (2020) 115801.
[35] R. Wannapob, P. Kanatharana, W. Limbut, A. Numnuam, P. Asawatreratanakul, C. Thammakhet, P. Thavarungkul, Affinity sensor using 3-aminophenylboronic acid for bacteria detection, Biosens. Bioelectron. 26 (2010) 357–364.
[36] X. Zhang, X. He, L. Chen, Y. Zhang, Boronic acid modified magnetic nanoparticles for enrichment of glycoproteins via azide and alkyne click chemistry, J. Mater. Chem. 22 (2012) 16520–16526.
[37] H. Wang, Z. Bie, C. Lü, Z. Liu, Magnetic nanoparticles with dendrimer-assisted boronate avidity for the selective enrichment of trace glycoproteins, Chem. Sci. 4 (2013) 4298–4303.
[38] J. Du, M. He, X. Wang, H. Fan, Y. Wei, Facile preparation of boronic acid-functionalized magnetic nanoparticles with a high capacity and their use in the enrichment of cis-diol-containing compounds from plasma, Biomed. Chromatogr. 29 (2015) 312–320.
[39] G. Francius, P. Polyakov, J. Merlin, Y. Abe, J.-M. Ghigo, C. Merlin, C. Beloin, J.F.L. Duval, Bacterial surface appendages strongly impact nanomechanical and electrokinetic Properties of *Escherichia coli* cells Subjected to osmotic stress, PLoS One 6 (2011), e20066.
[40] V.N. Nikitina, N.V. Zaryanov, E.E. Karyakina, A.A. Karyakin, Electropolymerization of 2-aminophenylboronic acid and the use of the resulting polymer for determination of sugars and oxyacids, Russ. J. Electrochem. 53 (2017) 312–317.
[41] V.N. Nikitina, N.V. Zaryanov, I.R. Kochetkov, E.E. Karyakina, A.K. Yatsimirsky, A.A. Karyakin, Molecular imprinting of boronate functionalized polyaniline for enzyme-free selective detection of saccharides and hydroxy acids, Sens. Actuators, B 246 (2017) 428–433.
[42] M. Matsushita, H. Kuramitz, S. Tanaka, Electrochemical oxidation for low concentration of aniline in neutral pH medium: Applications to the removal of aniline based on the electrochemical polymerization on a carbon fiber, Environ. Sci. Technol. 39 (2005) 3805–3810.
[43] M. Golabi, F. Kuralay, E.W.H. Jager, V. Beni, A.P.F. Turner, Electrochemical bacterial detection using poly(3-aminophenylboronic acid)-based imprinted polymer, Biosens. Bioelectron. 93 (2017) 87–93.

[44] J. Wu, R. Wang, Y. Lu, M. Jia, J. Yan, X. Bian, Facile preparation of a bacteria imprinted artificial receptor for highly selective bacterial recognition and label-free impedimetric detection, Anal. Chem. 91 (2019) 1027–1033.
[45] V.V. Malev, V.V. Kondratiev, Charge transfer processes in conducting polymer films, Russ. Chem. Rev. 75 (2006) 147–160.
[46] C. Erridge, E. Bennett-Guerrero, I.R. Poxton, Structure and function of lipopolysaccharides, Microb. Infect. 4 (2002) 837–851.
[47] D.E. Heinrichs, J.A. Yethon, C. Whitfield, Molecular basis for structural diversity in the core regions of the lipopolysaccharides of *Escherichia coli* and *Salmonella enterica*, Mol. Microbiol. 30 (1998) 221–232.
[48] P. Caffrey, P. Owen, Purification and N-terminal sequence of a subunit of antigen 43, a unique protein complex associated with the outer membrane of *Escherichia coli*, J. Bacteriol. 171 (1989) 3634–3640.
[49] I.R. Henderson, M. Meehan, P. Owen, Antigen 43, a phase-variable bipartite outer membrane protein, determines colony morphology and autoaggregation in *Escherichia coli* K-12, FEMS Microbiol. Lett. 149 (1997) 115–120.
[50] B. Heras, M. Totsika, K.M. Peters, J.J. Paxman, C.L. Gee, R.J. Jarrott, M.A. Perugini, A.E. Whitten, M.A. Schembri, The antigen 43 structure reveals a molecular Velcro-like mechanism of autotransporter-mediated bacterial clumping, Proc. Natl. Acad. Sci. Unit. States Am. 111 (2014) 457–462.
[51] A. Jacquot, C. Sakamoto, A. Razafitianamarahavo, C. Caillet, J. Merlin, A. Fahs, J.-M. Ghigo, J.F.L. Duval, C. Beloinc, G. Francius, The dynamics and pH-dependence of Ag43 adhesins' self-association probed by atomic force spectroscopy, Nanoscale 6 (2014) 12665–12681.
[52] P. Aprikian, G. Interlandi, B.A. Kidd, I.L. Trong, V. Tchesnokova, O. Yakovenko, M.J. Whitfield, E. Bullitt, R.E. Stenkamp, W.E. Thomas, E.V. Sokurenko, The bacterial fimbrial tip acts as a mechanical force sensor, PLoS Biol. 9 (2011), e1000617.
[53] A. Jacquot, C. Sakamoto, A. Razafitianamaharavo, C. Caillet, J. Merlin, A. Fahs, G. Ghigo, C. Beloin, J.F.L. Duval, G. Francius, Dynamic modulation of fimbrial extension and fimH-mannose binding force on live bacteria under pH changes: a molecular atomic force microscopy analysis, J. Biomed. Nanotechnol. 10 (2014) 3361–3372.
[54] L. Gao, X. Lu, H. Liu, J. Li, W. Li, R. Song, R. Wang, D. Zhang, J. Zhu, Mediation of extracellular polymeric substances in microbial reduction of hematite by *Shewanella Oneidensis* MR-1, Front. Microbiol. 10 (2019) 575.
[55] S.B. Subramanian, S. Yan, R.D. Tyagi, R.Y. Surampalli, Extracellular polymeric substances (EPS) producing bacterial strains of municipal wastewater sludge: isolation, molecular identification, EPS characterization and performance for sludge settling and dewatering, Water Res. 44 (2010) 2253–2266.
[56] J.R. Lawrence, G.D.W. Swerhone, U. Kuhlicke, T.R. Neu, In situ evidence for metabolic and chemical microdomains in the structured polymer matrix of bacterial microcolonies, FEMS Microbiol. Ecol. 92 (2016) 1–12.
[57] R. Sonohara, N. Muramatsu, H. Ohshima, T. Kondo, Difference in surface properties between *Escherichia coli* and *Staphylococcus aureus* as revealed by electrophoretic mobility measurements, Biophys. Chem. S5 (1995) 273–277.
[58] F. Gaboriaud, M.L. Gee, R. Strugnell, J.F.L. Duval, Coupled electrostatic, hydrodynamic, and mechanical properties of bacterial interfaces in aqueous media, Langmuir 24 (2008) 10988–10995.